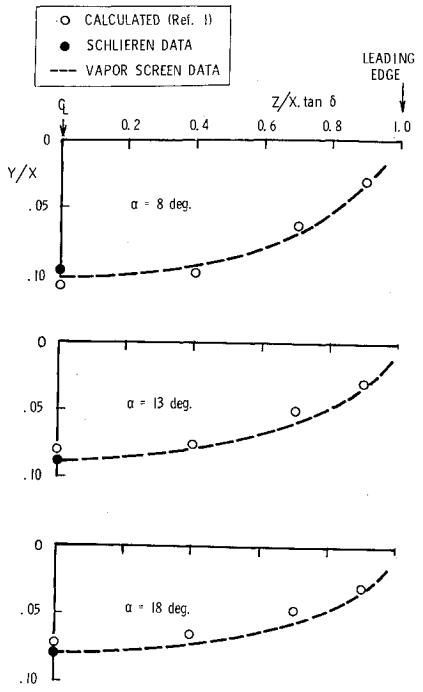

Fig. 2 Comparison of calculated and measured shock data.

It is expected that such agreement in the shock position between hot and cold tests would persist at points off the center plane.

The shock position in the center-plane and at several spanwise locations was calculated from the charts presented by Squire[1] for Mach 6.8 and ratio of specific heats 1.4. The computed points are compared with the shock shape traced off the vapor screen photographs, corrected for perspective distortion, in Fig. 2. Here again a generally good agreement is found in the range of incidence investigated.

The use of Squire's theory to check the experimental results requires comment. This theory has not been previously assessed experimentally for shock shape in published literature (except in the plane of symmetry by optical measurements, as in Ref. 2 where agreement similar to that found here was obtained at $M = 8.2$). However, it has been found to yield satisfactory predictions of spanwise pressure distribution over a variety of delta wing shapes in the Mach number range 2.47 to 8.6.[1] Squire's solution for the wing shock shape was used to calculate the interaction with the flap shock on a delta wing with trailing-edge flap at $M = 8.2$[3] and good agreement with experiment was obtained. Thus, it is felt that Squire's theory provides the shock shape for delta wings with reasonable accuracy.

While the data presented here is limited to one Mach number and model configuration, the schlieren results as well as theoretical calculations of this study suggest that the vapor screen technique is useful for quantitative shock information. A very simple experimental technique would then appear to be available for determining the hypersonic shock envelope of complex vehicle configurations.

References

[1] Squire, L. C., "Calculations of the Pressure Distribution on Lifting Conical Wings with Applications to the Off-Design Behavior of Wave Riders," AGARD Conference Prodeedings No. 30, 1968, pp. 11-1–11-21.

[2] Rao, D. M., "Hypersonic Control Effectiveness Studies on Delta Wings with Trailing-Edge Flap," Ph.D. thesis, 1970, Uni. of London, England.

[3] Rao, D. M., "Shock Interaction Effect on a Flapped Delta Wing at $M = 8.2$," *AIAA Journal*, Vol. 9, No. 5, May 1971, pp. 985–986.

A Comparison of Some Finite Element and Finite Difference Methods for a Simple Sloshing Problem

WEN-HWA CHU*
Southwest Research Institute
San Antonio, Texas

A. Introduction

BY a finite element method, we mean an application of a variational principle[1] and a quadrature formula for integration over each element. By a finite difference method, we mean the use of finite difference formulas derivable from a truncated Taylor series at the nodes. In the former method, equations at the nodes are obtained by "minimizing" the integral with respect to each independent generalized coordinate at the nodes.

Recently, Hunt[2] employed a second-order finite element formula which is derivable from Hamilton's principle, subject to a zero divergence condition (i.e., incompressible flow). A trapezoidal rule was implicitly used. Hunt's method is ingenious because only one normal displacement coordinate is required at each midpoint of the sides of the square element. But, before extending it to more general cases, it seems that a comparison of Hunt's method to other methods of computing fuel sloshing for a two-dimensional rectangular tank is worthwhile. Computation based on Hunt's method and two other methods will be given in this paper.

For heat conduction problems, analogous comparisons are given by Emery and Carson.[3] The subject of the present paper, however, is concerned with potential flow with a free surface.

B. Description of Methods

1. *Hunt's method (method I)*

For each element, there is a constraint of zero divergence, which therefore generates one dependent generalized coordinate and reduces the independent coordinates by one. From Hamilton's principle and trapezoidal rule, one finds (see Fig. 1).

$$2\bar{L} = \sum_e \tfrac{1}{2}\rho\omega^2 h^2[\zeta_+^2 + \zeta_-^2 + \xi_+^2 + \xi_-^2] \qquad (1)$$

which is to be minimized subject to the constraint condition that

$$\zeta_+ - \zeta_- + \xi_+ - \xi_- = 0 \qquad (2)$$

This process leads to an eigenvalue problem, where the eigenvalue is related to the natural frequency parameter and each eigenvector indirectly determines the respective free-surface mode shape.

2. *A simple finite difference method (method II)*

The governing differential equation is the well-known Laplace equation. The difference operator which is used at

Fig. 1 Generalized displacements of a square element; Hunt's method.

Received May 10, 1971. This investigation is supported by the Planning Council of Southwest Research Institute. The general study of the finite element method for fluids at SwRI was initiated by H. N. Abramson. Further, the programing assistance of H. Pennick is very much appreciated, as well as the technical editing by M. A. Sissung.

* Staff Scientist. Member AIAA.

Table 1 Comparison of natural frequency parameter and machine time (CDC-6400 computer); fractional error and absolute error

Mode	Method I		Method II		Method III		Exact value
	6 × 6	11 × 11	6 × 6	11 × 11	6 × 6	11 × 11	
1	−0.0609/1	−0.0189/1	−0.0822/1	−0.02940/1	0.0288/1	0.00782/1	3.1229
	−0.19086	−0.0591	−0.2576	−0.0919	0.089761	+0.024440	
2	−0.1778/1	0.0444/1	−0.244/1	−0.0967/1	0.0857/1	0.0296/1	6.2831
	−1.21596	−0.27836	−1.5304	−0.6070	0.534705	0.185495	
3	−0.3344/1	0.1668/1	−0.406/1	−0.180/1	0.1149/1	0.0582/1	9.4248
	−3.152	−1.5709	−3.80352	−1.69620	1.08142	0.54695	
4	−0.452/1	0.1938/1	0.1939/1	−0.266/1	0.0455/1	0.0852/1	12.5664
	−5.6748	−2.4318	2.4336	−3.34055	0.55859	1.06971	
5	...	0.267/1	...	−0.347/1	−0.0998/1	0.1027/1	15.7080
	...	−4.1609	...	−5.4415	−1.56582	1.61256	
6	...	−0.333/1	...	−0.419/1	...	0.1042/1	18.8495
		−6.2703	...	−7.8885	...	1.96286	
7	...	−0.396/1	...	−0.482/1	...	0.0854/1	21.9911
		−8.6862	...	−10.592	...	1.87649	
8	...	−0.453/1	...	−0.537/1	...	0.0444/1	25.1327
	...	−11.3497	...	−13.4936	...	1.1172	
9	...	−0.502/1	...	...	...	...	28.2743
	...	−14.2200	...	...	...	−0.5097	
10	...	...	...	...	...	...	31.4159
	...	...	...	...	...	−2.12163	
CP time (sec)	5.272	294.25	2.59	31.01	1.437	3.766	
PP time (sec)	3.687	3691.66	(7.61)	2.82	(2.546)	0.241	

the interior nodes is the simple H-operator.[4] On the wall, the equation $\partial\phi/\partial n = 0$ is approximated by three-point forward and backward formulas of second-order accuracy which, however, are inferior in accuracy to the central difference formula. On the flat free surface, we have

$$\omega^2\phi - g(\partial\phi/\partial n) = 0 \tag{3}$$

Again, a second-order backward formula is used for $\partial\phi/\partial n$-$(= \partial\phi/\partial z)$.

3. *A Finite element method based on velocity potential (method III)*

Let ϕ be the amplitude of velocity potential. For a periodic motion with $\rho = 1$,

$$2\bar{L}_e = \tfrac{1}{2}\int_D [(\partial\phi/\partial x)^2 + (\partial\phi/\partial z)^2]dS - \frac{g}{\omega^2}\int_F (\partial\phi/\partial n)^2 ds \tag{4}$$

For a rigid tank,

$$\delta(2\bar{L}_e) = [-\int_D \nabla^2\phi\delta\phi ds + \int_{\partial D} (\partial\phi/\partial n)\delta\phi ds] - (g/\omega^2)\int_F (\partial\phi/\partial n)\delta(\partial\phi/\partial n)ds \tag{5}$$

On the free surface, there is the condition that $\phi - (g/\omega^2)\partial\phi/\partial n$ = constant. The constant can be absorbed into the definition of ϕ; then $-(\omega^2 a/g)\phi + \partial\phi/\partial n^* = 0$, where $n^* = n/a$ and a = a characteristic length, say width. In the domain, $\nabla^2\phi = 0$. On the wall $\partial\phi/\partial n = 0$ which is a free boundary condition and no constraint needs to be imposed. We shall use central difference formulas and average for the derivative at centroid. If midpoints only are used, the interior equation is not Laplacian; hence, corner points are used. For the interior points (see Fig. 2a),

$$2\bar{L}_e = 2\bar{T}_e = \tfrac{1}{2}[(\phi_1 - \phi_2)^2 + (\phi_9 - \phi_3)^2] + \tfrac{1}{2}[(\phi_1 - \phi_9)^2 + (\phi_2 - \phi_3)^2] \tag{6}$$

$$\partial(2\bar{L}_e)/\partial\phi_9 = 4\phi_9 - \phi_3 - \phi_7 - \phi_1 - \phi_5 = 0 \tag{7}$$

which is the same as using the Laplace H-operator on ϕ. For the left side (see Fig. 2b),

$$4\phi_0 - 2\phi_4 - \phi_1 - \phi_3 = 0 \tag{8}$$

which is equivalent to using the H-operator with the extrapolated boundary point 2 and the central difference formula $(\partial\phi/\partial n)_0 = \phi_4 - \phi_2/2\Delta x$. Or, using Taylor's expansion to check this equation, we have

$$\phi_4 = \phi_0 + (h^2/2!)(\partial^2\phi/\partial x^2)_0,\ h = \Delta x = \Delta z,\quad (\partial\phi/\partial x)_0 = 0 \tag{9a,b,c}$$

$$\phi_1 = \phi_0 + (h/1!)(\partial\phi/\partial z)_0 + (h^2/2!)(\partial^2\phi/\partial z^2)_0 \tag{10}$$

$$\phi_3 = \phi_0 - (h/1!)(\partial\phi/\partial z)_0 + (h^2/2!)(\partial^2\phi/\partial z^2)_0 \tag{11}$$

$$4\phi_0 - 2\phi_4 - \phi_1 - \phi_3 = -[(\partial^2\phi/\partial x^2)_0 + (\partial^2\phi/\partial z^2)_0] = 0 \tag{12}$$

Similar expressions hold for the right side and the bottom of the tank. For the free surface (see Fig. 2c),

$$4\phi_0 - 2\phi_3 - \phi_2 - \phi_4 - 2h\frac{\omega^2}{g}\phi_0 = 0 \tag{13}$$

For the right upper corner (see Fig. 2d),

$$2\phi_0 - \phi_3 - \phi_2 - h\frac{\omega^2}{g}\phi_0 = 0 \tag{14}$$

Set $\omega = 0$ for the lower corners; the equation at the left upper corner is similar to that for the right upper corner. All noted equations can be checked by Taylor's series with the boundary conditions and differential equations. Therefore, this method is also a finite difference method. How-

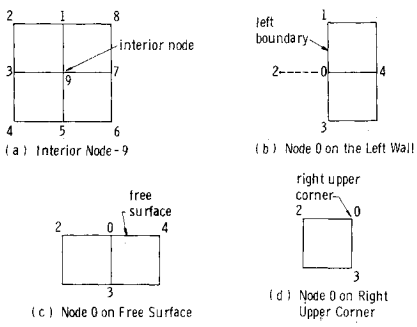

Fig. 2 Effective neighboring nodes for velocity potential.

ever, it is a more accurate method, with simpler derivation of the boundary conditions, than method II. Nevertheless, such simple representations of derivatives in the finite element method are limited to square, cubic or rectangular elements.

C. Numerical Result

1. *Hunt's example*

We used Hunt's example of a 4 × 6 element rectangle to check the programming of the Hunt's method. The results are in complete agreement with the published results.

2. *Square domain*

The results of the three methods applied to a square domain are given in Table 1. It can be seen that the finite element method based on ϕ using the central differences and the central averages is the most accurate, and also it is the simplest to program. Method III is faster than method II because the matrix inversion has been accomplished by breaking down the matrix to smaller submatrices and inverting one row at a time from the bottom up,† noting that the matrix inversion time for a medium size matrix is proportional to n^3. Method I for an 11 × 11 domain takes a very long machine time because of the apparent necessity to use disk storage outside the computer core, due to the presence of a large augmented matrix. Further, the long CP (Central Processor) time is due to the large eigenvalue problem that arises unless Hunt's intuitive method of eliminating the zero frequency modes is used.‡ For the latter, CP time could be greatly reduced while PP (Peripheral Processor) time would be further increased. Methods II and III have a steady motion mode which was excluded, and the 9th and 10th modes in the 11 × 11 case should not be taken seriously since these are the last two modes.

D. Conclusion

The finite element method based on the velocity potential ϕ with the central differences and the central averages is the most efficient of the three methods compared. However, a square, a cubic, or a rectangular domain is required before the central differences and the central averages can be applied. Since simple finite difference methods may be less accurate, it appears that a "machine transformation"§[5] combined with variational principles may be the most efficient for three-dimensional sloshing. It is noted that this approach may be comparable with the Khabbaz' method.[6] However, the quadrature formula given in Ref. 6 may not be optimum. Even for the first mode, the numerical value of the natural frequency undershoots the exact value as the mesh is refined. It is doubtful that the undershooting is due to round-off errors; it is probably a truncation error, the solution of which may not approach the exact solution in the limit. The proposed approach would be approximately a second-order process, provided that suitable mapping is employed.

References

[1] Zienkiewicz, A. C. and Cheung, Y. K., "The Finite Element Method in Structures and Continuum Mechanics," McGraw-Hill, New York, 1967.

[2] Hunt, D. A., "Discrete Element Structure Theory of Fluids," AIAA Paper 70-23, New York, 1970.

[3] Emery, A. F. and Carson, W. W., "Evaluation of Use of the Finite Element Method in Computation of Temperature," ASME Paper 69 WA/HT38, Nov. 16–20, 1969, Los Angeles, Calif..

[4] Milne, W. E., "Numerical Solution of Differential Equations," Wiley, New York, 1953, p. 131.

[5] Chu, W. H., "Development of General Finite Difference Approximation for a General Domain, Part I—Machine Transformation," SwRI Project IR 02-9034-01, Final Rept., Aug. 1970, *Journal Computational Physics*, to be published.

[6] Khabbaz, G. R., "Dynamic Behavior of Liquids in Elastic Tanks," LMSC 60-80-70-23, Aug. 1970, Lockheed Missiles & Space Co., Palo Alto, Calif.

† In method II, two-step inversion is used.

‡ This was used in the 6 × 6 case.

§ An abbreviated term for the numerical transformation using high speed computer.

A Higher Performance Electric-Arc-Driven Shock Tube

Wesley A. Menard
Jet Propulsion Laboratory, Pasadena, Calif.

Introduction

Simulation of Jupiter and Saturn atmospheric entry has been difficult[1] because entry velocities range from 25–48 km/sec. Shock tube velocities have been limited to about 15 km/sec.[2–4] The purpose of this Note is to report the development of an electric arc-driven shock tube which has increased shock velocity by a factor of three. The new driver has a conical internal design of small volume, and uses lightweight diaphragms. Data obtained from a 15.2-cm-diam driven tube show little shock wave attenuation. Shock velocities of 45 km/sec with test times in excess of 4 μ sec have been attained.

Shock Tube

Energy for the driver is supplied by a 100 capacitor storage system, rated at 290,000 joules when charged to 20,000 v. The new driver is shown schematically in Fig. 1 and is a modification of an earlier design.[5] The cathode is a 3.2-cm-diam cylinder made from Mallory 1000 (a sintered tungsten alloy). A hole in the cathode tip allows for pulling through the trigger wire. The anode is a 2.5-cm-wide, 7.7-cm-diam copper ring located 9.6 cm from the cathode. A conical teflon insert reduces the driver volume to 350 cm^3, and provides a fairly smooth internal contour from the cathode tip to the 15.2-cm-diam driven tube. The diaphragm is located on the downstream side of the anode ring. A 0.025-cm-diam stainless steel wire is strung across the opening, and attached to this wire is the trigger pull wire. In operation, pulling the trigger wire toward the cathode initiates the arc.

Mylar diaphragms (0.35 mm thick) are used to reduce diaphragm opening losses and to insure a fast opening time. Helium or hydrogen gas is supplied to the driver at a pressure (11.8 atm) 4% less than the static rupture pressure of the diaphragms. When the arc is struck, the trigger wires and the diaphragm immediately disintegrate. At high driver energies the copper anode could not hold the arc. Severe erosion on the surface of the stainless steel transition section indicated the arc had extended 7 cm beyond the diaphragm. Current measurements of the capacitor bank discharge show the arc burns for about 25 μsec. The driver gas can receive energy from the arc while in the driver, and as it expands down the tube.

Measurements

The most abundant elements in the atmospheres of Jupiter and Saturn are believed to be hydrogen and helium. For this reason the majority of shock tube runs were made in a mixture of 80% He and 20% H_2 (by volume).

Received April 28, 1971.
This research sponsored by NASA under contract NAS 7-100.

* Senior Research Engineer. Member AIAA.